Heliyon 10 (2024) e25573

Contents lists available at ScienceDirect

Heliyon

journal homepage: www.cell.com/heliyon

Research article

Disulfidptosis characterizes the tumor microenvironment and predicts immunotherapy sensitivity and prognosis in bladder cancer

Guizhen Pan [a,1,**], Huan Xie [b,1], Yeye Xia [a,c,*]

[a] Department of Radiation Oncology, The First Affiliated Hospital of Anhui Medical University, Hefei, China
[b] Department of Urology, The Third Affiliated Hospital of Southern Medical University, Guangzhou, China
[c] Department of Oncology, Chengdu Fifth People's Hospital, Sichuan, China

ARTICLE INFO

Keywords:
Disulfidptosis
Bladder cancer
Immune microenvironment
Bioinformatics
Tumor subgroups
Prognosis signature

ABSTRACT

Background: Bladder cancer (BLCA) is prone to metastasis and has poor prognosis with unsatisfactory treatment responsiveness. Disulfidptosis is a recently discovered, novel mode of cell death that is closely associated with human cancers. However, a comprehensive analysis of the relationship between disulfidptosis and BLCA is lacking. Therefore, this study aimed to explore the potential effect of disulfidptosis on BLCA and identify a biomarker for evaluating the prognosis and immunotherapy of patients with BLCA.

Material and methods: We acquired BLCA RNA sequencing data from The Cancer Genome Atlas Urothelial Bladder Carcinoma (TCGA-BLCA) cohort (containing 19 normal samples and 409 tumor samples) and the GES39281 cohort (containing 94 tumor samples) which were used for external validation of the signature. Initially, we performed unsupervised consensus clustering to explore disulfidptosis-related subgroups. We then conducted functional enrichment analysis on these subgroups to gain insights into their biological significance and evaluate their immunotherapy response and chemotherapy sensitivity. Next, we conducted Least Absolute Shrinkage and Selection Operator (LASSO) regression and multivariate Cox regression to construct a prognostic signature in the TCGA training set for prognosis-related differentially expressed genes (DEGs) in the disulfidptosis-related subgroups. Subsequently, we used a receiver operating characteristic (ROC) curve and independent prognostic analysis to validate the predictive performance of the signature in the TCGA testing and the GES39281 cohorts. Finally, we explored the therapeutic value of this signature in patients with BLCA, in terms of immunotherapy and chemotherapy.

Result: In this study, we obtained two subgroups: DRG-high (238 samples) and DRG-low (160 samples). The DRG-high group exhibited a poor survival rate compared to the DRG-low group and had a significant association with tumor grade, stage, and metastasis. Additionally, several pathways related to cancer and the immune system were enriched in the high-DRG group. Moreover, the DRG-high group exhibited higher expression of PD1 and CTLA4 and had a better response to immunotherapy in patients with both PD1 and CTLA4 positivity. Conversely, the DRG-high group was more sensitive to common chemotherapeutic agents. A prognostic signature

* Corresponding author.
** Corresponding author.
E-mail addresses: penguin2521@163.com (G. Pan), yeyexia18781735256@163.com (Y. Xia).
[1] Guizhen Pan and Huan Xie contributed equally to this study.

https://doi.org/10.1016/j.heliyon.2024.e25573
Received 28 July 2023; Received in revised form 13 January 2024; Accepted 29 January 2024
Available online 5 February 2024
2405-8440/© 2024 The Authors. Published by Elsevier Ltd. This is an open access article under the CC BY-NC-ND license (http://creativecommons.org/licenses/by-nc-nd/4.0/).

was created, consisting of *COL5A1*, *DIRAS3*, *NKG7*, and *POLR3G* and validated as having a robust predictive capability. Patients in the low-risk-score group had more immune cells associated with tumor suppression and better immunotherapy outcomes.
Conclusion: This study contributes to our understanding of the characteristics of disulfidptosis-related subgroups in BLCA. Disulfidptosis-related signatures can be used to assess the prognosis and immunotherapy of patients with BLCA.

1. Introduction

Bladder cancer (BLCA) is one of the most common urinary tract tumors, impacting over 4.3 million individuals worldwide annually and resulting in nearly 1.7 million fatalities [1]. For patients with non-muscle-invasive bladder cancer (NMIBCa), the primary treatment is transurethral resection of the bladder tumor (TURBT). By contrast, patients diagnosed with muscle-invasive BCa (miBCa) typically undergo multimodal treatment involving radical cystectomy and neoadjuvant chemotherapy [2–4]. Despite substantial

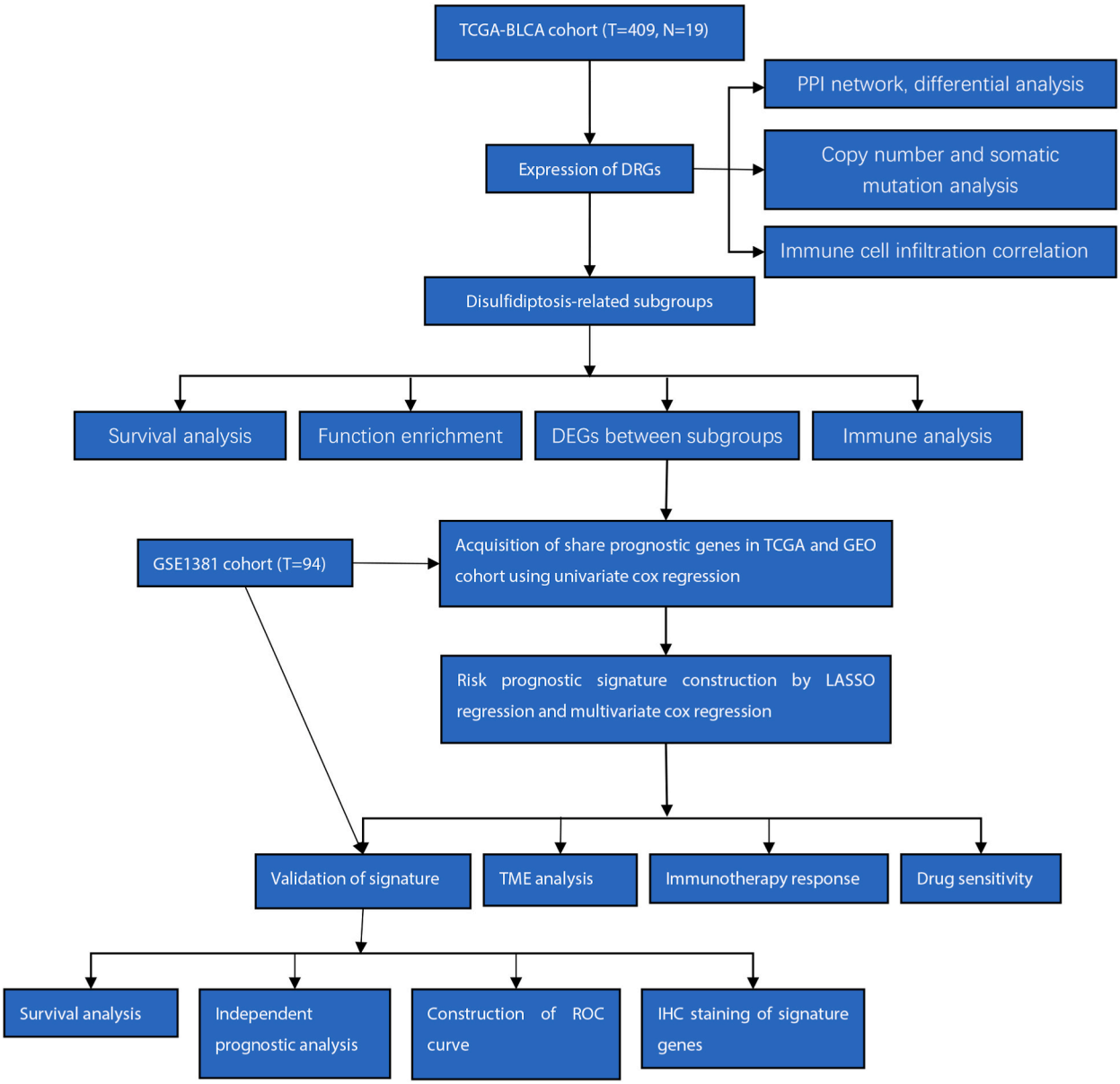

Fig. 1. Flow chart for the study analysis.

advancements in surgical and chemotherapeutic approaches in recent years, the rates of morbidity, mortality, and cancer recurrence in patients with BLCAs have not improved significantly.

In recent years, the development of cancer genomics and revival of immunotherapy have led to the study of different classifications of BLCA subgroups to guide personalized treatment. Zhou et al. identified the molecular subtypes mediated by apoptosis-related genes that promote treatment outcomes in patients with BLCA [5]. Zheng et al. (2022) identified CD93-associated molecular subtypes of BLCA that are particularly relevant for guiding immunotherapeutic approaches [6]. Although these studies have elucidated the significant role of BLCA subtypes in personalized therapy, there is a lack of diversity among different molecular subtypes when examined from the perspective of disulfidptosis.

Accidental cell death (ACD) and regulated cell death (RCD) are the two common types of cell death [7]. Most cancer treatment strategies are engineered to specifically target malignant cells while sparing their non-malignant counterparts. Distinct lethal subroutines within the RCD paradigm exert varying effects on tumor progression and therapeutic responsiveness. Unlike ACD, RCD is controlled by specific signal transduction pathways that can be modulated by pharmacological or genetic interventions. The most extensively studied types of RCD are apoptosis, pyroptosis, necroptosis, and ferroptosis, all of which have distinct molecular mechanisms [8,9]. Disulphidroptosis is a recently discovered mode of cell death, distinct from other forms of cell death, characterized by the accumulation of cysteine and abnormal disulfide bond formation. Disulfidptosis occurs in *SLC7A11*^{high} cells under low glucose conditions Under these circumstances, intracellular cystine accumulates excessively owing to the depletion of NADPH, thereby fostering the formation of abnormal disulfide bonds, particularly within cytoskeletal proteins such as actin. Consequential structural damage leads to disintegration of the actin cytoskeleton, and ultimately, cell death [10]. Recent studies have underscored the close association between disulfidptosis and various human cancers and its pivotal role in tumor suppression, offering promising avenues for targeted therapeutic approaches to cancer treatment [11,12]. However, limited research has focused on the molecular profile of disulfidptosis in BLCA. Therefore, it is imperative to explore the genetic and molecular characteristics related to disulfidptosis to augment our understanding of the disease mechanisms implicated in BLCA and to offer fresh insights into potential therapeutic interventions.

Using data obtained from The Cancer Genome Atlas (TCGA) and the Gene Expression Omnibus (GEO) databases, we categorized BLCA into two disulfidptosis-related subgroups and conducted a comprehensive analysis of the subgroups, including overall survival (OS), pathological characteristics, immune microenvironment, immunotherapy responsiveness, and sensitivity to immunotherapy and chemotherapy. We further established a prognostic signature and assessed the prognosis, immune microenvironment, immunotherapy, and drug sensitivity in patients with BLCA.

2. Materials and methods

2.1. Data Acquisition and organization

Fig. 1 illustrates the study process. We collected 428 BLCA samples from TCGA (https://portal.gdc.cancer.gov/), consisting of 409 tumor samples and 19 normal samples. Clinical information, copy number variants (CNV), and somatic cell mutation data were obtained from the TCGA. Of the 409 patients with BLCA, 398 with complete survival information were randomly divided into training (N

Table 1
Clinical information of the TCGA cohort.

TCGA cohort	Entire cohort (N = 398)	Testing cohort (N = 119)	Training cohort (N = 279)
Age			
≤65	158	50	108
>65	240	69	171
Gender			
0	102	29	73
1	296	90	206
Stage			
I	2	1	1
II	127	43	84
III	138	41	97
IV	131	34	97
T			
0	1	1	0
1	3	1	2
2	126	40	86
3	207	51	156
4	61	26	35
M			
0	368	108	260
1	30	11	19
N			
0	258	79	179
1	50	12	38
2	83	24	59
3	7	4	3

= 279) and testing (N = 119) cohorts at a ratio of 70:30 (Table 1). In addition, we downloaded the GSE39281 (https://www.ncbi.nlm.nih.gov/geo/query/acc.cgi) cohort of 94 patients with BLCA from the GEO as an external validation cohort (Table 2). Disulfidptosis related genes (DRGs) were extracted from previous studies.

2.2. Protein-protein interactions (PPI) and differential analysis

To investigate the intercommunication of these DRGs, protein-protein interaction (PPI) analysis was performed using the STRING website (https://cn.string-db.org/), and the resulting PPI network was visualized using Cytoscape [13]. Prognosis-related DRGs were identified by univariate Cox regression analysis.

2.3. Generation of disulfidptosis-associated subgroups and function enrichment

Based on prognosis-related DRGs, consensus clustering using the k-means method was used to identify subgroups associated with DRGs using the ConsensuClusterPlus package [14]. After that, the reliability of the clustering was verified by the R package "ggplot2" using the uniform manifold approximation (UMAP) method [15]. Kaplan-Meier (K-M) curve of OS was plotted to explore the prognostic differences between subgroups using "Survival" and "survminer" packages, and then Chisq test was performed to analyze the correlation between subgroups and clinicopathological factors. Statistical significance was set at $p < 0.05$ [16].

To explore the underlying biological mechanisms contributing to intergroup differences, Gene Set Variation Analysis (GSVA) was conducted using the "GSVA" package in R software to identify enriched pathways within each subgroup [17]. Additionally, a differential analysis was conducted using the "limma" package, with the filtering criteria set at $p < 0.05$, FDR <0.01, and $|\log2FC| \geq 1$, to identify differentially expressed genes (DEGs) between subgroups [18]. Subsequently, Gene Ontology (GO) and Kyoto Encyclopedia of Genes and Genomes (KEGG) analysis was performed using the "clusterProfiler" package of R software using the same he filtering criteria [19,20].

2.4. Immune microenvironment analysis and immunotherapy

Based on the TCGA-BLCA expression profile, the "estimate" R package was applied to calculate the immune score and stromal score of each patient with BLCA [21]. We initially estimated the differences in the immune, stromal, and estimated scores between DRG subgroups using the Wilcoxon test. Next, single sample gene set enrichment analysis (ssGSEA) analysis was performed using the R package "GSVA" to assess and quantify the degree of immune cell infiltration in each sample, with a filtering criterion set at $p < 0.05$ [17,22]. Subsequently, the "limma" package was used to analysize the expression levels of *PD1* and *CTLA4* between subgroups. In addition, the immunophenotype scores (IPS) of patients with BLCA from The Cancer Immunome Atlas (TCIA) (https://tcia.at/) were used to explore the role of DRG subgroups in immunotherapy responses [23]. Statistical significance was determined when differences between subgroups exhibited a p-value of less than 0.05.

2.5. Drug sensitivity analysis

Using the RNA expression profile of TCGA-BLCA, we calculated the half-maximal inhibitory concentrations (IC50) of antitumor drugs commonly used in the treatment of patients with BLCA using the "pRophetic" package of R software, and assessed the IC50 levels between different subgroups using the Wilcoxon test and screening criteria at $p < 0.05$ [24].

2.6. Construction and validation of a prognosis signature for disulfidptosis

Based on the DEGs of the DRG subgroups, prognosis-related genes were screened using univariate Cox regression in TCGA cohort. In TCGA training cohort, least absolute shrinkage and selection operator (LASSO)regression and univariate Cox regression analyses were performed to construct a prognosis signature. The signature formula constructed based on multivariate Cox regression analysis is as follows:

Table 2
Clinical information of the GEO cohort.

GSE39281 cohort (N = 94)	number
Stage	10
0	
1	5
2	45
3	28
4	5
Visceral M	
0	59
1	34

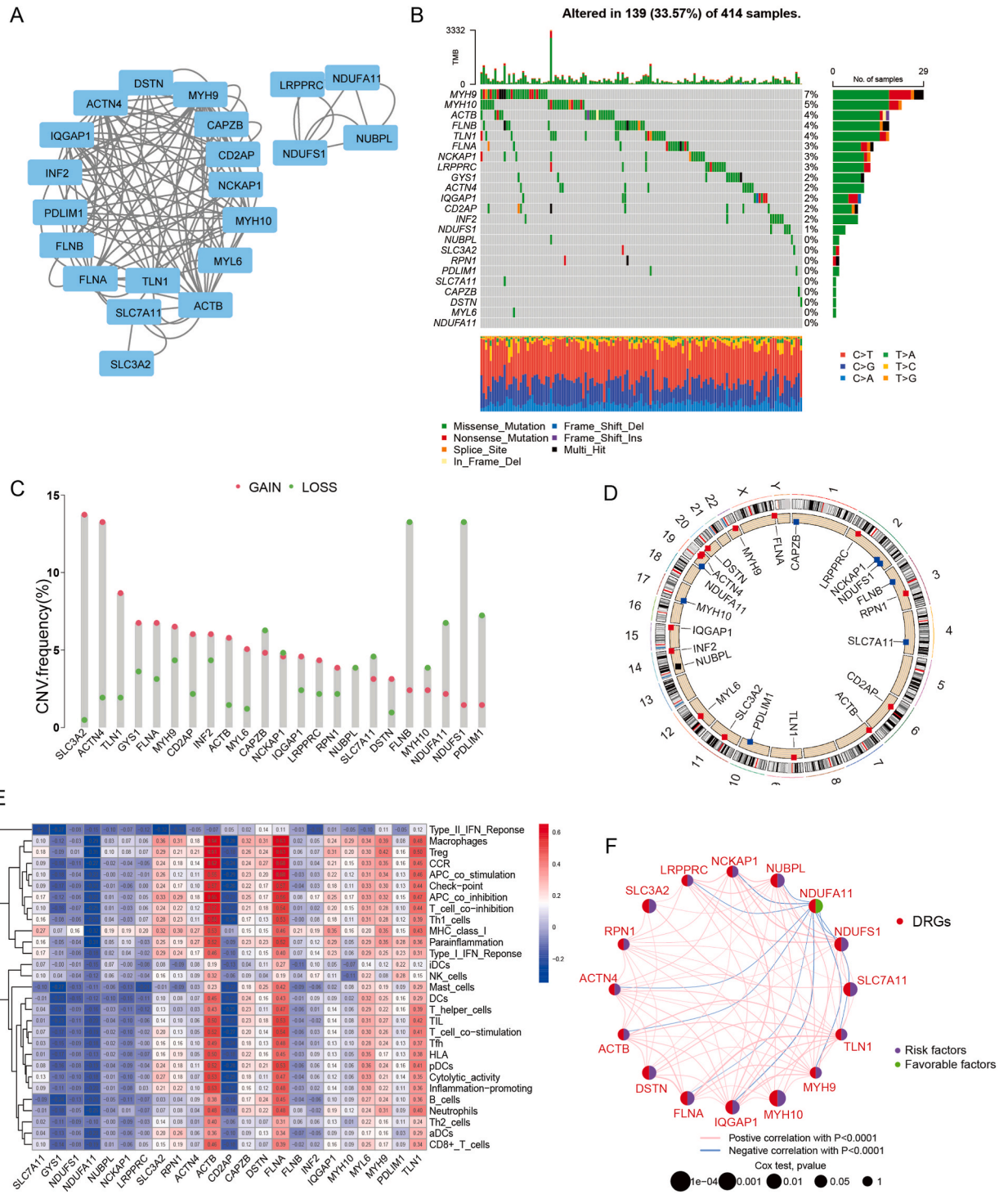

Fig. 2. Expression characteristics of DRGs in BLCA. (A) PPI network diagram of DRGs. (B) Somatic mutation waterfall plot of 23 DRGs. (C) CNV of 23 DRGs in TCGA-BLCA. (D) Localization and alteration of 23 DRGs in the chromosome region. (E) Correlation heat map of 23 DRGs and immune cells. (F) Prognosis-related genes in DRGs.

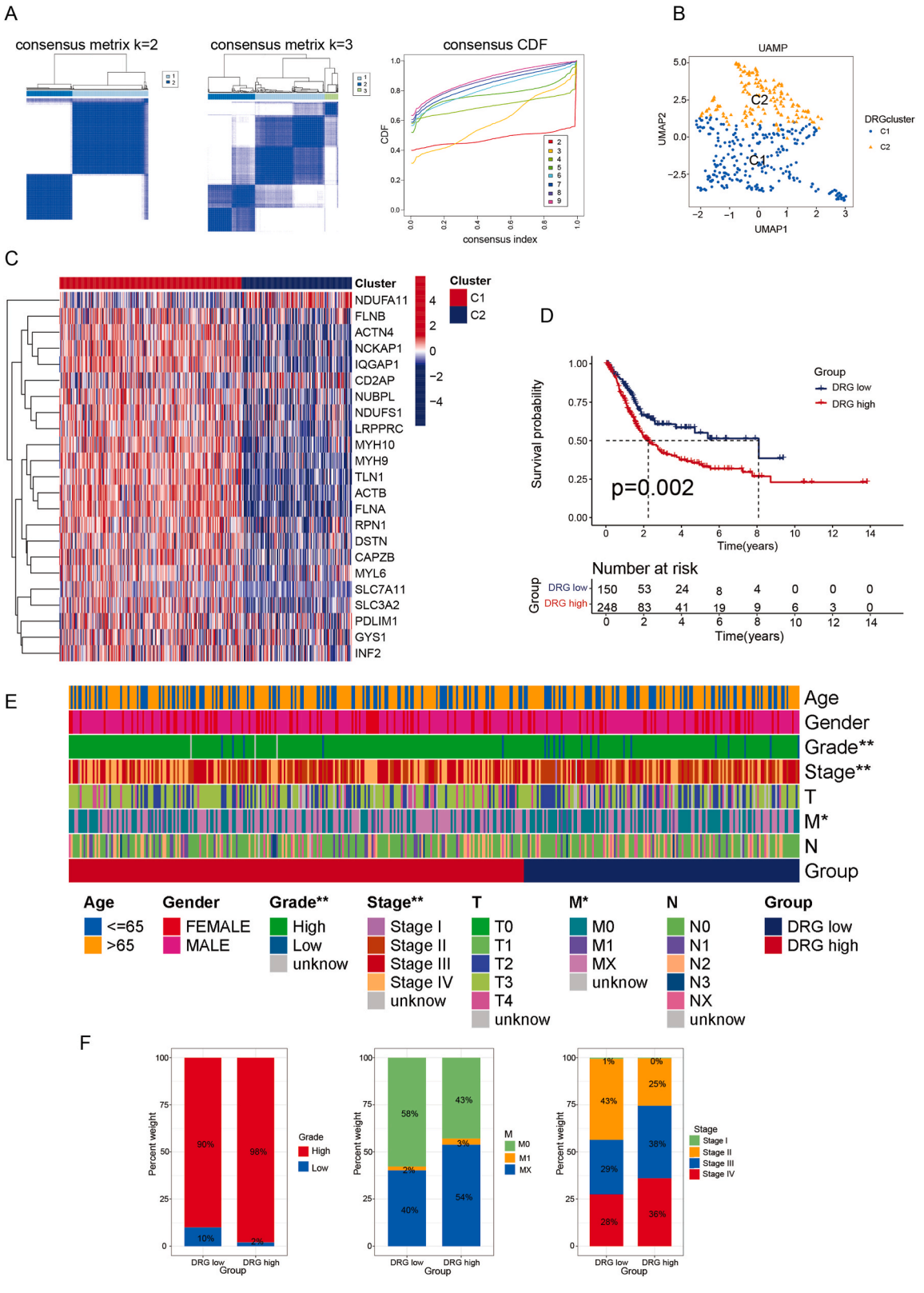

(caption on next page)

Fig. 3. Subgroups of BLCA based on DRG expression. (A) Consensus matrix was obtained by applying consensus clustering when k = 2 and 3. When k = 2, the slope of the CDF curve is the lowest. (B) UMAP was used to distinguish the two subgroups based on DRG expression levels. (C) DRG expression heat maps in two subgroups. (D) K-M curve of OS in the two subgroups. (E)Clinicopathologic features of the two subgroups. (F) Proportional bar charts for each stage, grade, and metastasis in the DRG-low and -high groups. *, $p < 0.05$; **, $p < 0.01$; ***, $p < 0.001$.

$$Riskscore = \sum_{n}^{1} \beta_1 \times Exp(Gene_1) + \beta_2 \times Exp(Gene_2) ... \beta_n \times Exp(Gene_n)$$

The risk score of each patient with BLCA was calculated using the signature formula. Based on the median risk score, patients with BLCA were divided into high-risk and low-risk groups. In TCGA training cohort, K-M curve of OS was plotted to explore the prognostic value of the signature, and Receiver Operating Characteristic (ROC) curves were constructed to assess the predictive performance of the signature. In addition, univariate and multivariate independent prognostic analyses were performed to identify whether the risk score was an independent prognostic factor for the survival of patients with BLCA. This signature was also validated in TCGA and GSE39281 cohorts.

2.7. Immune analysis and drug sensitivity analysis of prognosis signature

Immune cell infiltration was calculated for each individual based on seven currently popular algorithms (XCELL, TIMER, QUANTISEQ, MCPCOUNTER, EPIC, CIBERSORT−ABS, CIBERSORT) [25,26]. The "limma" package and Wilcox test was then used to calculate the correlation between risk scores and the abundance of various immune cell infiltration. The TME characteristics of the signature and their potential impact on immunotherapy were also analyzed. The R package "OncoPredict," with 198 drugs, was used to predict the in vivo drug response in patients of two risk groups [27].

2.8. Expression validation and localization of risk genes

Using IHC staining data from the Human Protein Atlas database (HPA, https://www.proteinatlas.org/), bladder tumor and normal tissue specimens were used to validate the expression of signature genes [28]. The Tumor Immune Single-Cell Hub (TISCH; http://tisch.comp-genomics.org), a large-scale online single-cell [29], was used to investigate the expression of the signature genes in various immune cells.

2.9. Statistical analyses

The R software (version 4.2) was used for all data analyses. The Wilcoxon test was used to compare two groups. The chi-square test was used to assess the relationship between subgroups and clinicopathological factors. A Pearson's correlation analysis was also performed. The "limma" package was used to screen subgroups of DEGs and the "ConsensuClusterPlus" package was used for unsupervised clustering analysis. The "GSVA" package was applied for GSVA and the "clusterProfiler" package for enrichment analysis. The "pRophetic" and "OncoPredict" package was carried out for drug sensitivity analysis. "Survival" and "survminer" were used for survival analysis. "ggplot2," "pheatmap," and "ggpubr" packages were used for plotting. In all statistical results, $p < 0.05$ and FDR <0.01 indicates statistical significance.

3. Result

3.1. Protein-protein interaction (PPI) and expression characteristics of DRGs

As shown in the PPI network diagram (Fig. 2A), the DRGs were closely related. The mutation landscape, as depicted in the waterfall plot, revealed that the majority of the 23 DRGs were mutated in BLCA, including *MYH9* (7 %), *MYH10* (5 %), *ACTB* (4 %), *FLNB* (4 %), *TLN1* (4 %), *FLNA* (3 %), *NCKAP1* (3 %), *LRPPRC* (3 %), *GYS1* (2 %), *ACTN4* (2 %), *IQGAP1* (2 %), *CD2AP* (2 %), and *INF2* (1 %) (Fig. 2B). We further explored the copy number analysis of DRGs and found that most of the 23 DRGs had increased copy numbers, except for *CAPZB*, *NCKAP1*, *NUBPL*, *SLC7A11*, *FLNB*, *MYH10*, *NDUFA11*, *NDUFS1*, *PDLIM1* in BLCA. (Fig. 2C and D). In the immune cell infiltration correlation heat map, it was evident that GYS1, NDUFA11, and CD2AP were negatively correlated with immune cell infiltration. In contrast, ACTB, FLNA, TLN1, MYL6, and MYH9 positively correlated with immune cell infiltration (Fig. 2E). Univariate Cox regression analysis of 23 DRGs revealed 16 prognosis-related genes (Fig. 2F).

3.2. Generation of disulfidptosis-related subgroups

To better explore the role of DRGs in BLCA, we performed unsupervised clustering analysis based on 16 prognosis-related DRGs. The results showed that TCGA-BLCA cohort could be effectively stratified into two distinct subgroups when k = 2. (Fig. 3A). Furthermore, the UAMP assay confirmed a clear separation of the two subgroups (Fig. 3B). Interestingly, the expression of almost all of DRGs was significantly higher in cluster 1, whereas it was notably lower in cluster 2. As a result, we designated cluster 1 as the "DRG-high group" and cluster 2 as the "DRG-low group" (Fig. 3C). Additionally, the K-M curve of OS demonstrated a poorer prognosis in the

DRG-high group (Fig. 3D). Furthermore, the DRG-high group exhibited a close correlation with worse tumor grade, stage, and metastasis (Fig. 3E–F). These findings strongly suggest that disulfidptosis-related subgroups have a predictive value for the prognosis of patients with BLCA.

3.3. Functional enrichment of disulfidptosis-related subgroups

To explore the potential mechanisms underlying the disulfidptosis-related subgroups, we first performed a GSVA. As shown in Fig. 4A and Supplementary materials 1, the DRG-high group exhibited significant enrichment in pathways related to the cytoskeleton and cell migration, including regulation of the actin cytoskeleton, focal adhesions (FA), extracellular matrix (ECM), and Cell Adhesion Molecules (CAMs). Furthermore, tumor-related pathways, such as the JAK-STAT signaling pathway, Toll-like receptor signaling pathway, and VEGF signaling pathways, were prominently upregulated in this group. Additionally, immune-related pathways, including cytokine-cytokine receptor interactions, primary immunodeficiency, natural killer cell-mediated cytotoxicity, chemokine signaling pathways, and B cell and T cell receptor signaling pathways, were also significantly enriched. Next, we identified 2352 differentially expressed genes (DEGs) through differential analysis, with 257 down-regulated and 2095 genes up-regulated (Fig. 4B and Supplementary materials 2). Gene Ontology (GO) analysis revealed that the top three biological processes (BPs) were positive regulation of cytokine production, positive regulation of cell adhesion, and external encapsulating structure organization. For cellular components (CC), the top three categories were the collagen-containing extracellular matrix, external side of the plasma membrane,

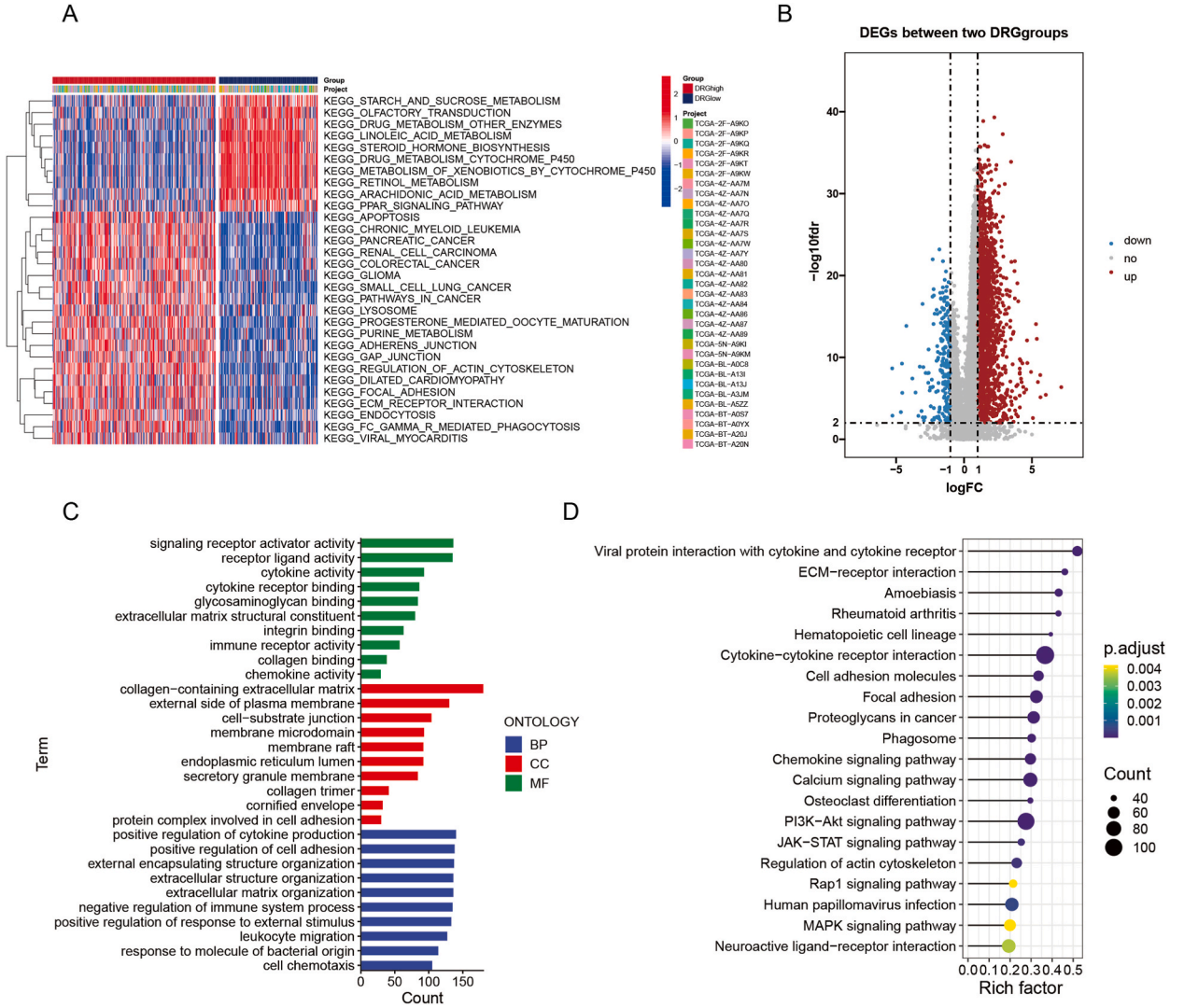

Fig. 4. Differential and enrichment analyses of subgroups. (A) Differences in pathway activity between the two different subgroups based on GSVA scores. (D) Volcano map of DEGs in the two subgroups. (C) GO analysis of DEGs in the two subgroups. (D) KEGG analysis of DEGs in the two subgroups.

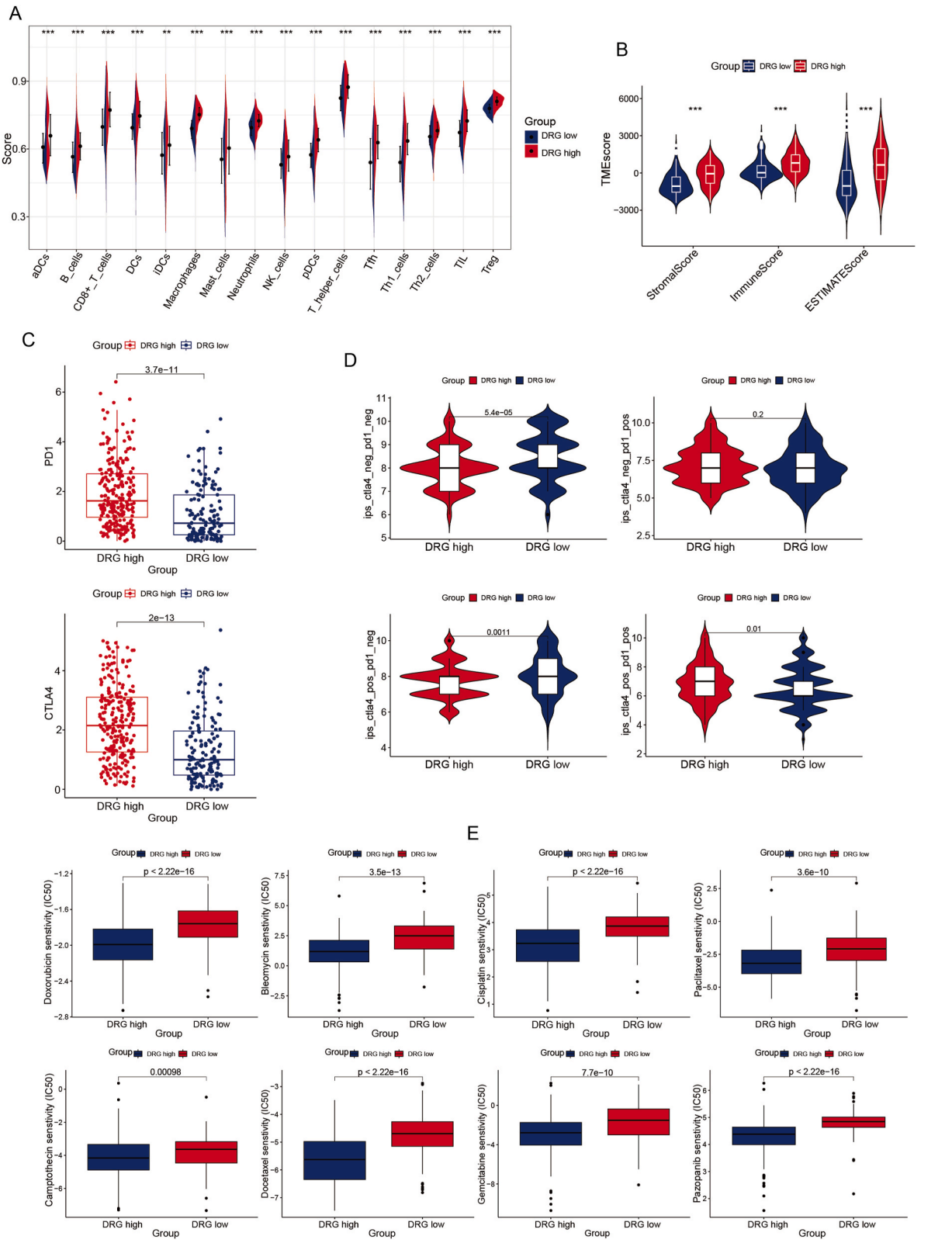

(caption on next page)

Fig. 5. Immune landscape of the two subgroups (A) Differential analysis of immune cells in ssGSEA. (B) TME scores, including immune, stromal, and estimate scores. (C) Comparison of *PD1* and *CTLA4* expression between subgroups. (D) The treatment effects of four immunotherapy strategies, including anti-*CTLA4* alone, anti-*PD1* alone, no medication, and combined medication was evaluated in the disulfidptosis-associated subgroups. (E) Sensitivity analysis of common chemotherapeutic agents (doxorubicin, bleomycin, rapamycin, mitomycin. cisplatin, docetaxel, gemcitabine, pazopanib camptothecin, and paclitaxel) in the disulfidptosis-associated subgroups. *, $p < 0.05$; **, $p < 0.01$; ***, $p < 0.001$.

and cell-substrate junction. Regarding molecular functions (MF), the top three were receptor-ligand activity, signaling receptor activator activity, and cytokine activity (Fig. 4C). KEGG analysis further enriched 54 pathways, with the top five pathways being the cytokine-cytokine receptor interaction, PI3K-Akt signaling pathway, neuroactive ligand-receptor interaction, calcium signaling pathway, and focal adhesion.

3.4. Immune microenvironment analysis

Our investigation of the immune microenvironment revealed distinct patterns within the disulfidptosis-related subgroups. First, the DRG-high group had significantly higher TME scores, encompassing immune, stromal, and estimated factors than the reference group (Fig. 5B). Similarly, ssGSEA analysis highlighted that an increase in various immune cells infiltrated the DRG-high group, in contrast to the DRG-low group (Fig. 5A). Furthermore, the DRG-high group displayed higher expression of *CTLA4* and *PD1*, indicating an increased potential to evade the immune system of the host organism (Fig. 5C). Notably, our immunotherapy analyses showed that patients in the DRG-high group gained a more pronounced benefit relative to patients in the DRG-low group when subjected to combined treatment with *PD1* and *CTLA4* inhibitors (Fig. 5D). These findings collectively emphasize the intricate interplay between the immune microenvironment composition, immune cell infiltration, and the expression of key immune checkpoint molecules, highlighting potential avenues for targeted therapeutic interventions.

3.5. Drug sensitivity analysis

Bladder cells are highly sensitive to chemotherapy. For patients with advanced BLCA in good physical condition, the preferred standard chemotherapy is based on cisplatin regimens such as MVAC, HD-MVAC, and GC. Second-generation drugs include gemcitabine combined with cisplatin and cisplatin combined with paclitaxel. Targeted angiogenesis agents such as bevacizumab and sunitinib. EGFR inhibitors. Molecular targeted drugs play a significant role in a small number of individuals [30,31]. Drug sensitivity analysis showed that the DRG-high group was more sensitive to common chemotherapeutic agents, including doxorubicin, bleomycin, rapamycin, mitomycin C, cisplatin, docetaxel, gemcitabine, pazopanib, camptothecin, and paclitaxel (Fig. 5E).

3.6. Construction and validation of disulfidptosis related prognosis signature

142,849Out of the 2352 DEGs initially identified, only 1772 were found in the GSE39281 cohort. We applied Univariate Cox regression analysis to the 1772 DEGs in both TCGA and GSE39281 cohorts and then obtained 55 prognosis-related genes shared by both cohorts for the construction of a prognostic signature (Supplementary materials 3). In the TCGA training cohort, LASSO regression selected nine genes for multivariate Cox regression, and ultimately, four genes (containing COL5A1, DIRAS3, NKG7, POLR3G) were chosen to construct a prognostic signature (Fig. 6A–B and Supplementary materials 4). The risk score formula for the signature was determined using multivariate Cox regression as follows:

$$Riskscore = 0.14 \times Exp(COL5A1) + 0.28 \times Exp(DIRAS3) - 0.23 \times Exp(NKG7) + 0.30 \times Exp(POLR3G)$$

The correlation heat map demonstrated a close association between the signature genes and DRGs (Fig. 6C). In TCGA training cohort, risk score curves and point plots depicting patient survival status revealed a significant association between elevated risk scores in patients with BLCA and unfavorable prognoses. The K-M curve of OS also demonstrated that patients in the high-risk score group had a poorer prognosis than patients in the low-risk score group ($p < 0.001$), indicating the promising prognostic value of the signature. Univariate (risk score <0.001, HR = 1.835 (1.501–1.231)) and multivariate independent prognostic analyses (risk score <0.001, HR = 1.563 (1.249–1.954)) confirmed that the risk score was an independent prognostic factor for BLCA. The 1-, 3-, and 5-year AUC values from the ROC curves were 0.705, 0.698, and 0.667, respectively, implying a reasonably robust predictive performance of the signature (Fig. 6D–H). The results of the risk score curves and point plots depicting patient survival status in the TCGA testing and GSE39281 cohorts were consistent with those in the TCGA training cohort (Figs.. 7A and 8A). Additionally, the K-M curve of OS in TCGA testing ($p = 0.007$) and GSE39281 ($p = 0.032$) cohorts demonstrated the relevance of the high-risk score group and poorer prognosis (Figs.. 7B and 8B). Univariate independent prognostic analysis in TCGA testing (risk score = 0.015, HR = 1.184 (1.034–1.357)) and GSE39281 (risk score = 0.001, HR = 1.652 (1.223–2.231)) cohorts, combined with multivariate independent prognostic analysis in TCGA testing (risk score = 0.007, HR = 1.230 (1.060–1.429)) and GSE39281 (risk score = 0.007, HR = 1.559 (1.130–2.151)), verified the risk score as an independent predictor of BLCA (Fig. 7D–E and Fig. 8D–E). In agreement with the TCGA training cohort, the 1-, 3-, and 5-year AUC values were 0.703, 0.721, and 0.684 in the TCGA testing cohort and 0.679, 0.741, and 0.788 in the GSE39281 cohort, respectively, validating the fairly stable predictive capability of the signature (Figs.. 7C and 8C).

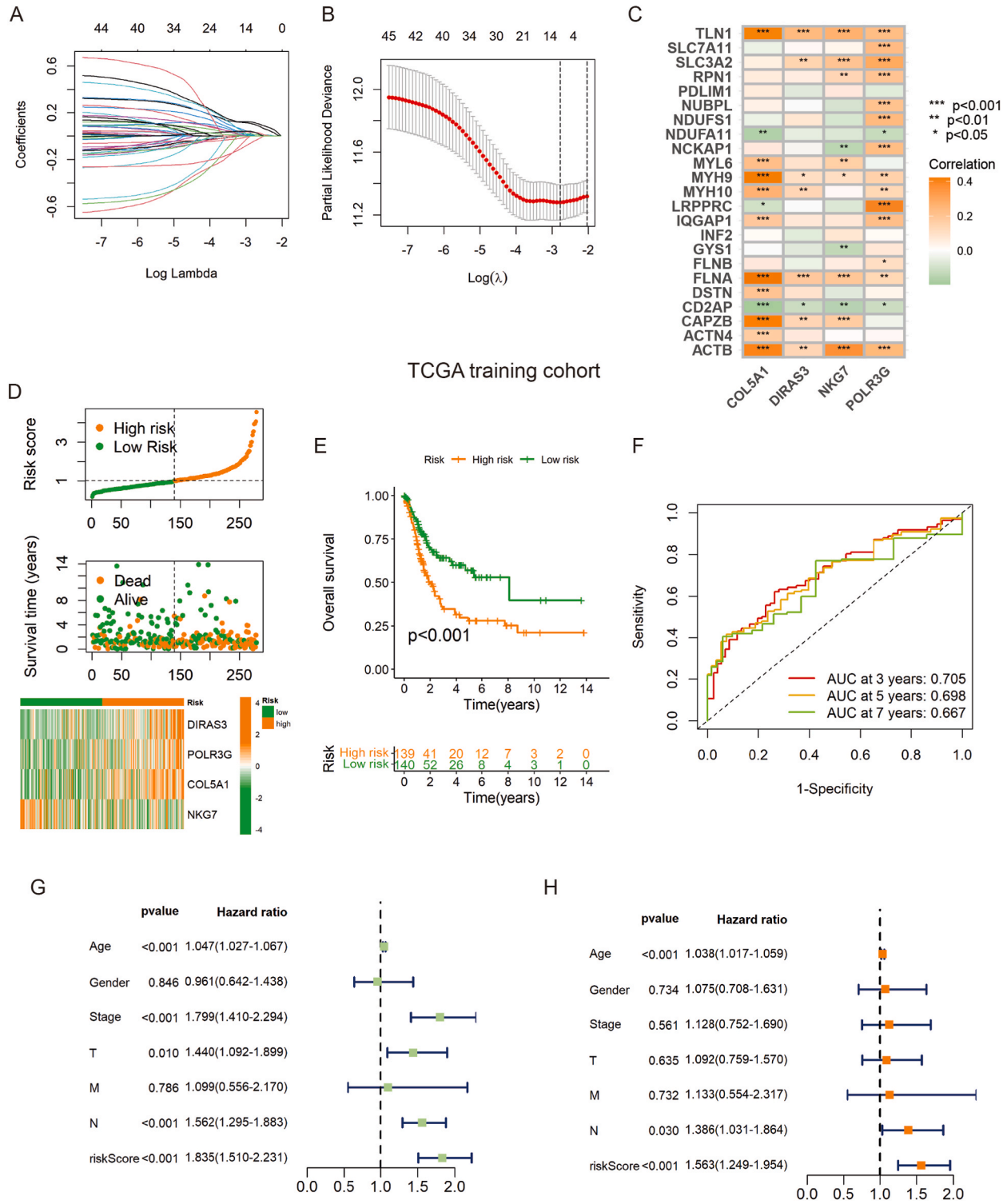

Fig. 6. Construction of prognosis signature in the TCGA training cohort. (A) LASSO regression analysis. (B) Cross-validation in LASSO regression. (C) Correlation heat map of risk genes and DRGs. (D) Risk score curves, risk state point maps, and risk gene expression heat maps in the TCGA training cohort. (E) K-M curve of OS In TCGA training cohort. (F) 1-, 3-, and 5-year ROC curve of risk score in the TCGA training cohort. (G) Univariate and (H) multivariate Cox regression analysis in the TCGA training cohort. *, $p < 0.05$; **, $p < 0.01$; ***, $p < 0.001$.

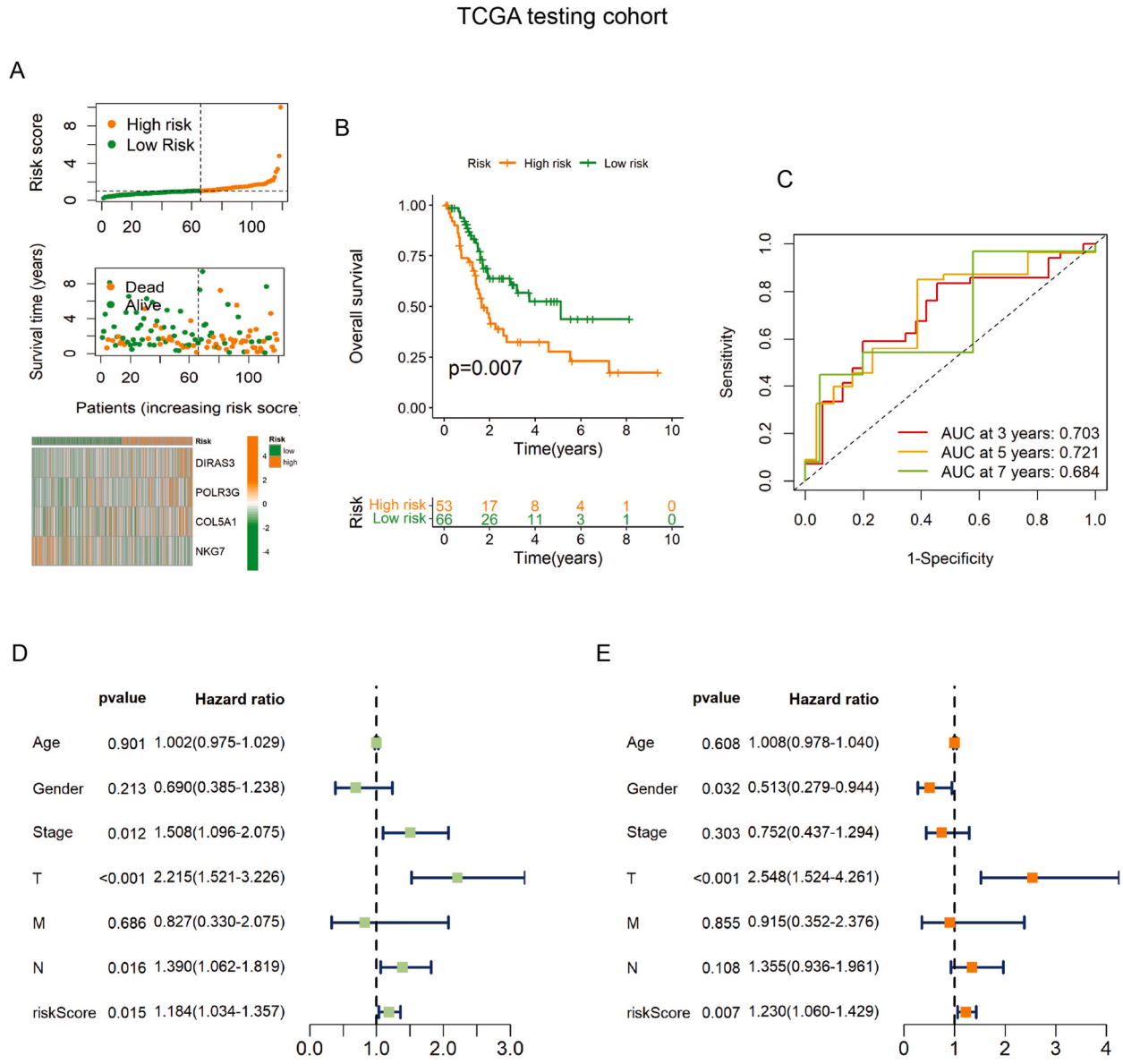

Fig. 7. Validation of the prognosis signature in TCGA testing cohort. (A) Risk score curve, risk state point map, and risk gene expression heat map. (B) K-M curve of OS in the TCGA testing cohort. (C) 1-, 3-, and 5-year ROC curves of risk score. (D) Univariate and (E)multivariate Cox regression analyses.

3.7. Immune landscape and drug sensitivity analysis of prognostic signature

In the immune infiltration bubble map based on the seven algorithms, the immune cells attacking the tumor, including CD8 + and CD4 + T cells, were significantly and negatively correlated with the risk score. However, immune cells associated with tumor progression, including cancer-associated fibroblasts and T2 macrophages, were significantly and positively correlated with the risk score (Fig. 9A). This implies that patients with high scores are less resistant to tumors. In addition, in the TME analysis, the high-risk score group had a higher score for stromal cells and a lower score for immune cells compared to the corresponding low-risk score group (Fig. 9B). Among the four immunotherapy cohorts, patients with low-risk scores had better outcomes (Fig. 9C). Drug sensitivity analysis revealed that some common drugs used in patients with BLCA, such as Epirubicin, Gemcitabine, Oxaliplatin, and Palbociclib, were more effective in low-risk patients (Fig. 9D).

3.8. Expression and localization of signature genes

As shown by the HIC staining data for DIRAS3, POLR3G and COL5A1, the expression of COLA5 and POLR3G was higher in the

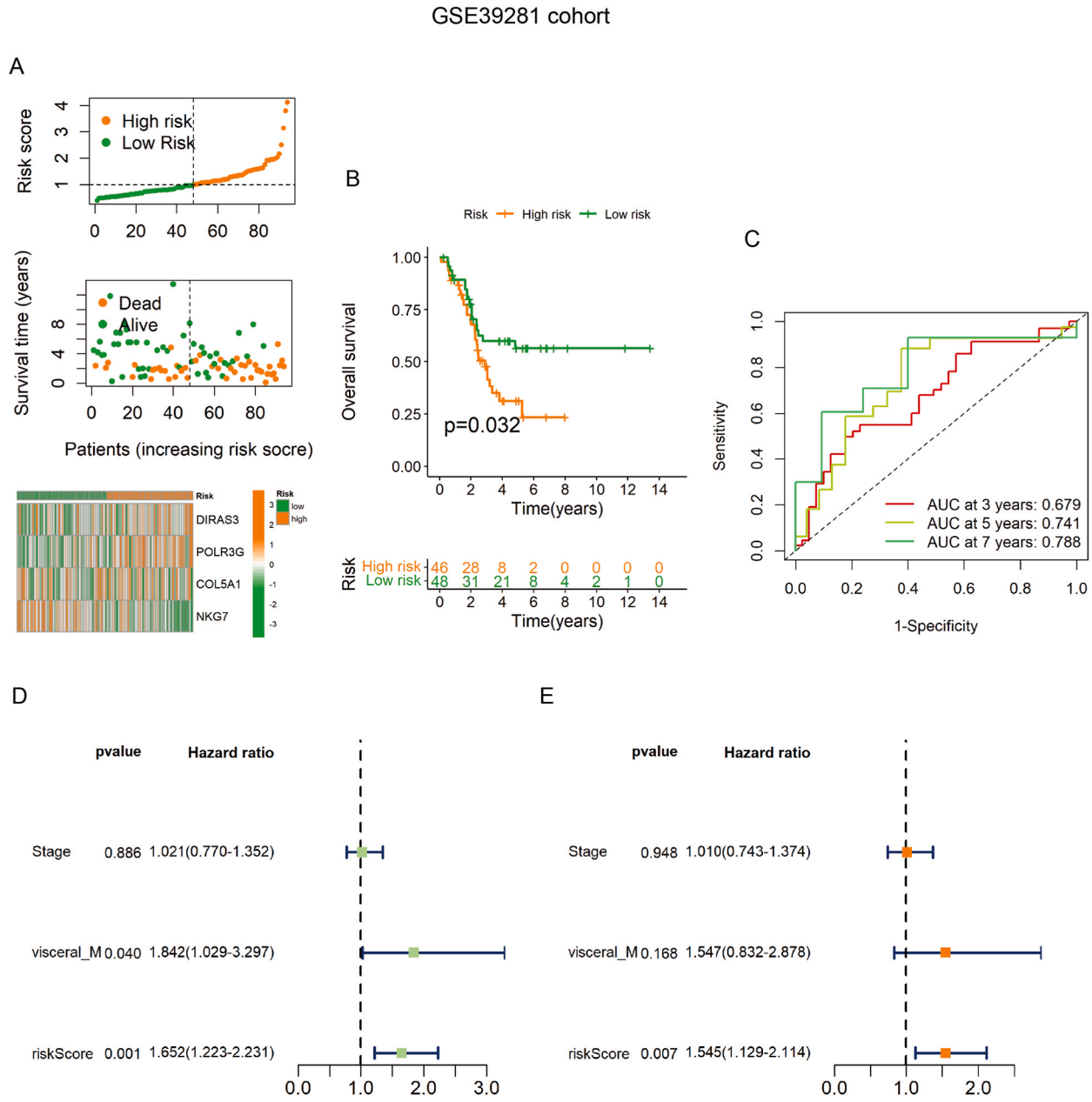

Fig. 8. Validation of the prognosis signature in the GSE39281 cohort. (A) Risk score curve, risk state point map, and risk gene expression heat map. (B) K-M curve of OS in the TCGA testing cohort. (C) 1-, 3-, and 5-year ROC curves of risk score. (D) Univariate and (E) multivariate Cox regression analyses.

tumor tissue specimen than in the normal tissue specimen (Fig. 10 A and C). Conversely, the expression of DIRAS3 was lower in the tumor tissue specimen than in the normal tissue specimen (Fig. 10 B).

We conducted a comparative analysis of the expression of these four genes in immune cells using single-cell RNA-sequencing profiles from three datasets: GSE13001 (patients with no therapy), GSE149652 (patients undergoing chemotherapy), and GSE145281_aPDL1 (patients receiving immunotherapy). Our findings revealed that *DIRAS3* expression was low only in patients who underwent chemotherapy. *POLR3G* and *COL5A1* showed low expression in all patient groups except those who received no therapy. Notably, *NKG7* displayed low expression in patients with no therapy but exhibited high expression in patients who received chemotherapy or immunotherapy, suggesting that NKG7 expression is linked to alterations in the immune microenvironment (Fig. 11A–C).

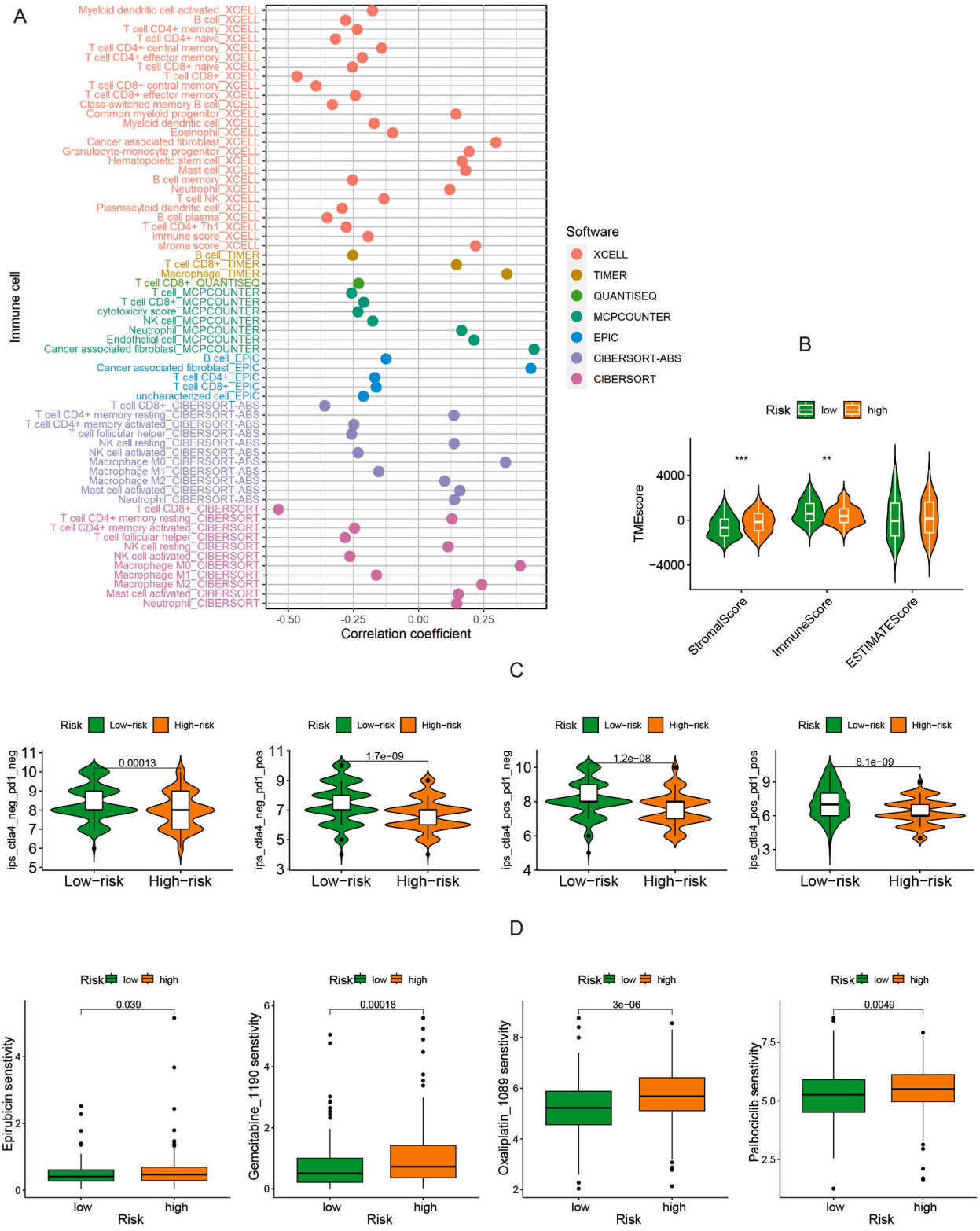

Fig. 9. Immune microenvironment analysis and drug sensitivity assessment. (A) immune cell bubble of risk groups. (B) Comparison of TME scores between high-and low-risk groups. (C) Differences in treatment response in the four immunotherapy cohorts in two subgroups. (D) Sensitive drugs in the two risk groups. *, $p < 0.05$; **, $p < 0.01$; ***, $p < 0.001$.

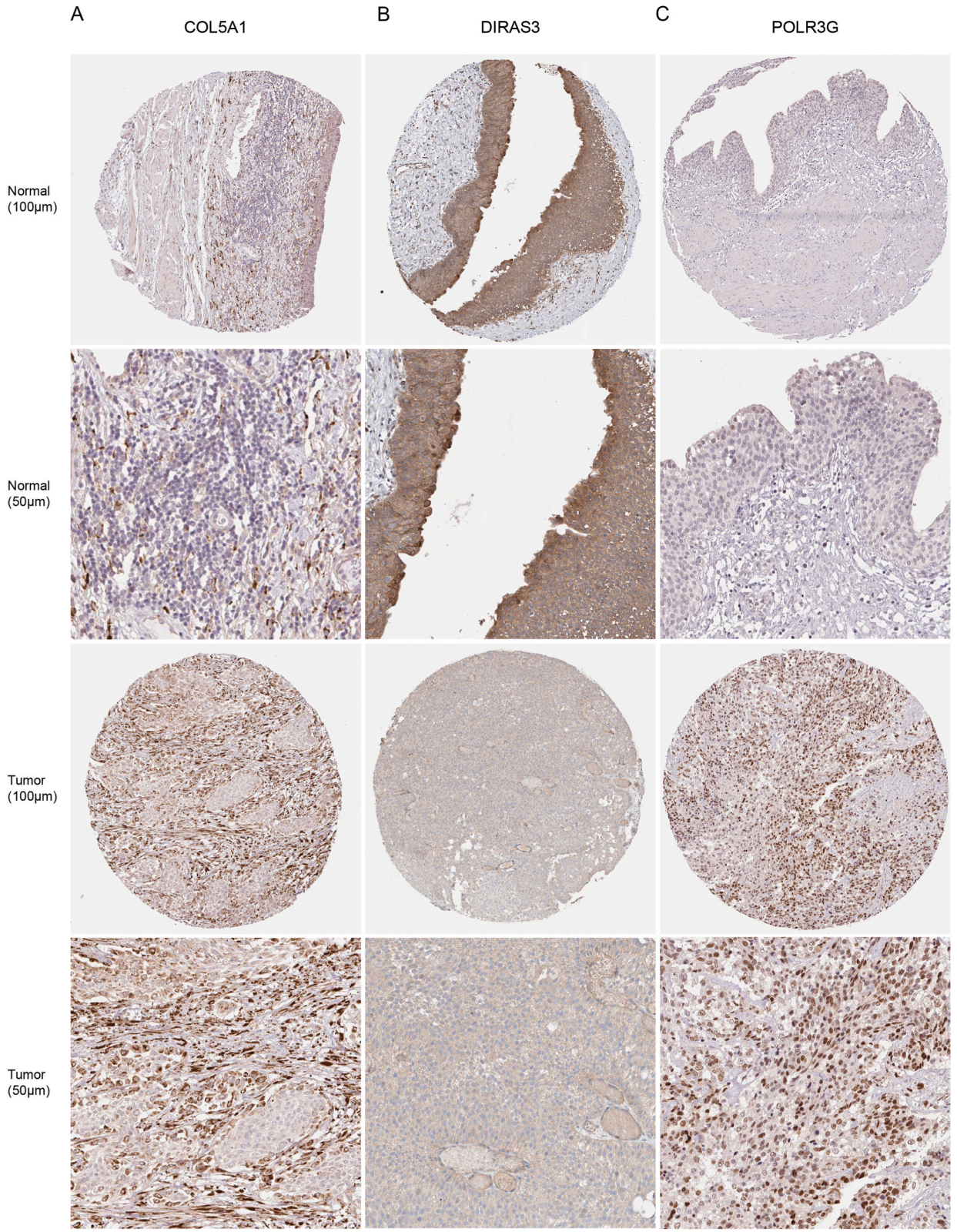

Fig. 10. Analysis of signature proteins expression in tumor and normal tissue specimens using IHC staining data from HPA. (A) the expression level of COL5A1 in tumor and normal tissue specimens. (B) the expression level of DIRAS3 in tumor and normal tissue specimens. (C) the expression level of POLR3G in tumor and normal tissue specimens.

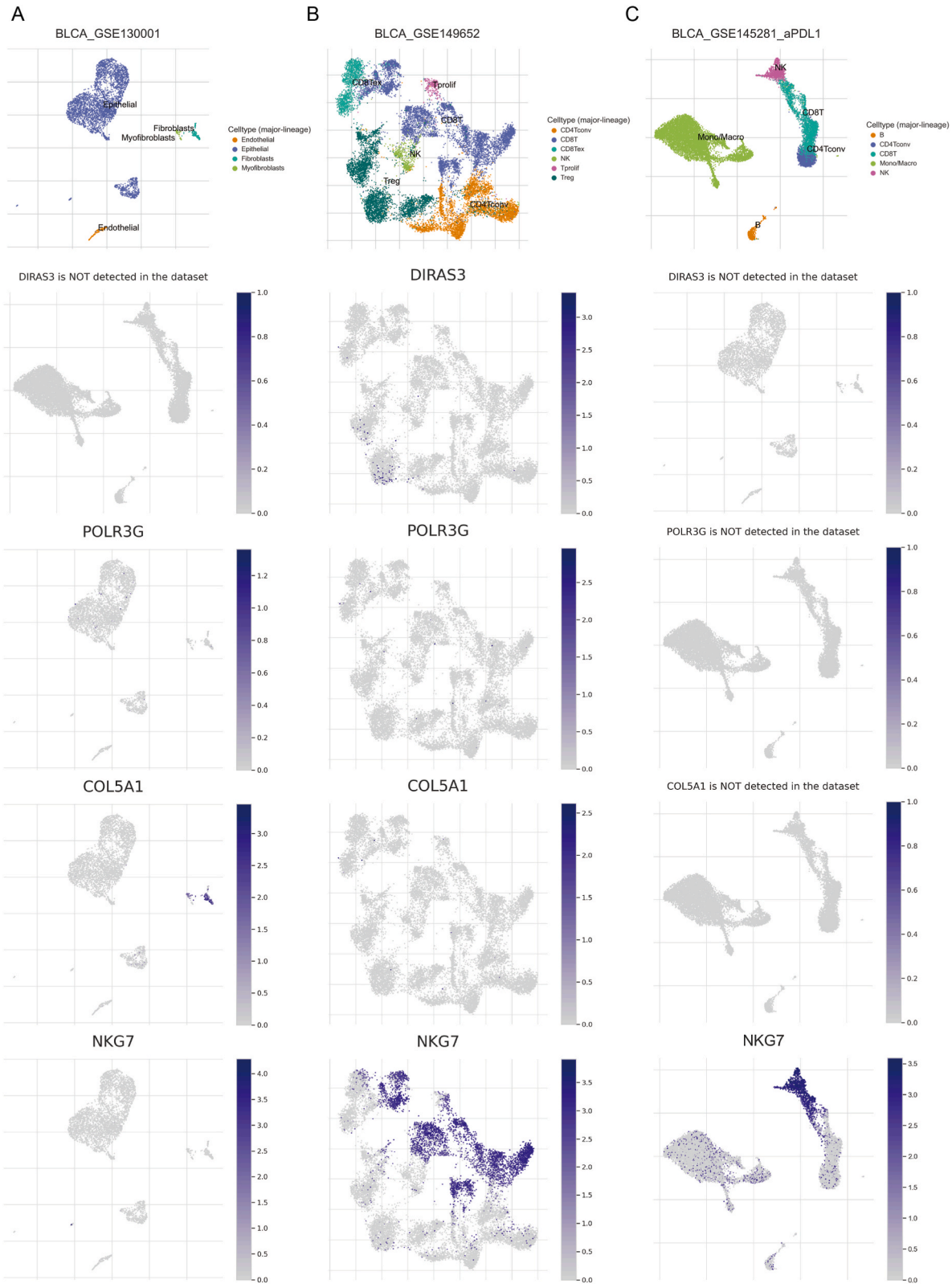

Fig. 11. Expression of the four signature genes in three single-cell datasets of BLCA. (A) Expression of the four signature genes in GSE13001 (patients with no therapy). (B) expression of four signature genes in GSE149652 (patients undergoing chemotherapy). (C) expression of four signature genes in and GSE145281_aPDL1 (patients receiving immunotherapy).

4. Discussion

Disulfidptosis is a new form of cell death caused by abnormal disulfide bond formation due to glucose starvation in *SLC7A11*^{high} cells. Rac-WRC-mediated lamellipodia formation, a key target for disulfide bonding among actin cytoskeleton proteins, promotes disulfidptosis. Under conditions of glucose starvation, the actin cytoskeleton of the affected cells exhibited an abnormal morphology, with contractions around the cell edges and the collapse of lamellipodia. Glycogen synthase (*GYS1*) and various genes involved in mitochondrial oxidative phosphorylation (such as *NDUFS1*, *NDUFA11*, *NUBPL*, and *LRPPRC*) are disulfidptosis suppressors whose inactivation synergizes with glucose starvation to induce cell death. Conversely, *SLC7A11*, *SLC3A2*, *RPN1*, and *NCKAP1* are activators required for disulfidptosis. These findings may provide a novel therapeutic strategy for suppressing tumor progression by enhancing disulfidptosis. However, studies on the potential role of disulfidptosis in bladder lacking. Therefore, our study aimed to explore the influence of disulfidptosis-related genes in BLCA, as well as their relationship with the immune microenvironment, to construct a prognostic signature for clinical prognosis evaluation and personalized treatment.

In the present study, patients with BLCA were systematically divided into two subgroups, namely high or low DRG groups, using unsupervised cluster analysis based on 16 prognostic DRGs. The K-M curve of OS showed that the prognosis of the DRG-high group was worse than that of the DRG-low group ($p = 0.002$). Simultaneously, the high-DRG group exhibited significant associations with advanced tumor grades, stages, and a higher incidence of metastatic spread. Functional enrichment analyses, including GSVA and KEGG, revealed that several actin cytoskeletal protein-, tumor-, and immune-related pathways were enriched in DRG-high group. Regarding the immune landscape, disulfidptosis-related subgroups exhibited distinctly different immune microenvironments. The high-DRG group displayed increased infiltration of various immune cell types and overexpression of immune checkpoint molecules, including *PD1* and *CTLA4*, compared to the low-DRG group. When *PD1* inhibitors were used in combination with *CTAL4* inhibitors, the high DRG group showed significantly better immunotherapy efficacy. Subsequently, based on the prognosis-related DEGs of the two DRG groups, four genes (containing *DIRAS3*, *POLR3G*, *COL5A1*, *NKG7)*were selected by LASSO regression and multivariate Cox regression to construct a prognostic signature. The K-M curve of OS indicated a worse prognosis in the high-risk group. Independent prognostic and ROC curve analyses in both TCGA and GEO cohorts confirmed the strong predictive performance of this signature. High-risk scores positively correlated with tumor-associated immune cell infiltration and predicted poorer outcomes with immunotherapy.

In the univariate Cox regression analysis for BLCA, 16 DRGs were associated with prognosis. These included the favorable factor *NDUFA11* and the risk factors *NCKAP1*, *SLC7A11*, *SLC3A2*, *LRPPRC*, *MYH9*, *MYH10, ACTN4*, *RPN1*, *ACTB*, *DSTN*, *FLNA*, *IQGAP1*, *TLN1*, *NDUFS1*, and *NUBPL*. *NDUFA11* is a subunit of complex I involved in mitochondrial oxidative phosphorylation [32]. As a disulfidptosis suppressor, it exhibited higher expression in the DRG-low group. *NCKAP1*, encoding Nck-associated protein 1 and a component of the WAVE regulatory complex (WRC), demonstrated its importance as its knockdown inhibited the migration of rectal cancer [33]. *SLC3A2* is a transmembrane protein that functions as a heterodimeric chaperone for amino acid transport proteins (such as *SLC7A5* and *SLC7A11*) and has been associated with cancer progression [34]. *RNP1* encodes ribonucleoprotein 1, a major component of the oligosaccharyltransferase (OST) complex that plays a crucial role in N-linked glycosylation. Research has shown that the knockdown of RNP1 inhibits the in vitro proliferation and invasion of breast cancer cells and induces apoptosis through the activation of endoplasmic reticulum stress [35]. *SLC7A11*, *NCKAP1*, *SLC3A2*, and *RPN1*, the critical activators of disulfidptosis, were highly expressed in the DRG-high group. *NDUFS1* and *NUBPL* are implicated in mitochondrial oxidative phosphorylation, and their mutations lead to impaired oxidative phosphorylation, resulting in mitochondrial diseases [36–38]. Although *NDUFS1*, *NUBPL*, and *LRPPRC* are suppressors of disulfidptosis, they were highly expressed in DRG-high group. *MYH9*, *MYH10*, *ACTN4*, *ACTB*, *FLNA* and *TLN1*, they are actin cytoskeletal proteins that produce abnormal disulfide bonds during disulfidptosis. Collectively, our results indicate that the DRG-high group, characterized by elevated expression of key DRGs, exhibited a robust association with disulfidptosis and may predispose patients to disulfidptosis.

Functional analyses were performed to elucidate the underlying mechanisms contributing to the differences between the two subgroups. GSVA analysis suggested that numerous pathways related to the cytoskeleton and cell migration were upregulated in the DRG-high group, including regulation of the actin cytoskeleton, focal adhesions, ECM, and CAMs. Focal adhesions are complex assemblies of plasma membrane-associated macromolecules that bind to the surrounding ECM via integrin receptors and are physically linked to the actin cytoskeleton through the recruitment of numerous FA-associated proteins [39]. CAMs are a large family of cell surface proteins that mediate attraction or repulsion between the ECM, stroma, and other cancer cells [40]. These signalling pathways have been shown to be involved in cell migration and cancer metastasis [41,42]. Moreover, focal adhesions and the ECM have been reported to be associated with tumor tolerance to chemotherapy and radiotherapy and may serve as ideal therapeutic targets [42]. Enrichment of these cytoskeleton-related pathways in the DRG-high group was consistent with the high expression of DRGs in this group. In addition, several pathways involved in tumorigenesis and tumor progression were upregulated. It can be speculated that the activation of these pathways is a reason for the poor prognosis in the DRG-high group. Interestingly, numerous immune-related pathways were also upregulated, prompting further investigation of the differences in the immune microenvironment between subgroups.

Immunotherapy is an innovative therapy that enhances the immune system by modulating the immune microenvironment so that immune cells can attack and remove tumor cells at several important nodes [43]. Immunotherapy is one of the most important treatments for patients with advanced BLCA; however, only a fraction of patients benefit from immunotherapy [44]. Individual differences in tumor progression exist due to heterogeneity in the tumor microenvironment [45]. Therefore, it is necessary to develop activation strategies that target the immune microenvironment based on the different immune escape mechanisms in the TME [46,47]. In our study, we observed distinct immune microenvironment patterns within disulfidptosis related subgroups. The DRG-high group

exhibited a significant increase in immune cell infiltration, including $CD8^+$ or cytotoxic T lymphocytes (CTL), NK cells, and Th1cells, which mainly play a role in killing and inhibiting tumor development in the TME [48]. Additionally, we noted elevated expression levels of *PD1* and *CTLA4* in the DRG-high group, implying that tumors in this subgroup possess a heightened ability to evade the immune system. Analysis of the immunotherapy cohort showed that patients in the DRG-high group treated with PD-1 inhibitors alone displayed a higher immunotherapeutic response than those in the DRG-low group; however, this difference was not statistically significant. Notably, the combination of *PD-1* and *CTLA-4* inhibitors demonstrated a significantly enhanced immunotherapeutic response in the DRG-high group compared with the DRG-low group. To enhance clinical management, we developed a prognostic signature based on the DEGs within the two DRG subgroups. This signature serves as a valuable tool for immunotherapy. Notably, patients with high-risk scores demonstrated an elevated presence of tumor-associated immune cell infiltration. Furthermore, we observed a significantly enhanced response to immunotherapy in the low-risk group compared to that in the high-risk group. These findings underscore the utility of our prognostic signature in facilitating personalized treatment strategies for patients.

Although our study successfully identified disulfidptosis-associated subgroups with distinct immune microenvironment patterns in BLCA, constructed a prognostic signature, and conducted both internal and external validations, it is important to acknowledge its limitations. First, the external validation dataset consisted exclusively of progressive BLCA cases, which may have introduced a potential bias into the results. Furthermore, our study lacked further validation through in vitro and in vivo experiments, which we intend to pursue in future studies.

5. Conclusions

We identified two disulfidptosis-related subgroups in BLCA that had different prognoses and immune microenvironments as well as different sensitivities to immunotherapeutic and chemotherapeutic agents. In addition, we constructed a disulfidptosis-related prognostic signature for predicting prognosis and response to immunotherapy and chemotherapy in patients with BLCA. These findings offer valuable insights into prognostic analysis and the potential for personalized treatment strategies in patients with BLCA.

Funding

Not applicable.

Consent for publication

The authors declare no conflicts of interest.

Ethics approval and consent to participate

Not applicable.

Data availability statement

The original contributions of this study are included in the article/supplementary material section. Further inquiries can be directed to the corresponding authors. The public data cohorts analyzed in this study can be found in TCGA (https://portal.gdc.cancer.gov/) and GEO (https://www.ncbi.nlm.nih.gov/geo/).

CRediT authorship contribution statement

GP and YX conceived the study and HX and YX performed the literature search and data collection. GP and HX contributed to the data analysis and drafting of the manuscript. GP revised the draft. All authors contributed to and approved the manuscript.

Declaration of competing interest

The authors declare no known financial interests or personal relationships that could have influenced the work reported in this paper.

Acknowledgments

The authors thank Mohammad Mofatteh for his contribution to the language revision of the manuscript.

Appendix A. Supplementary data

Supplementary data to this article can be found online at https://doi.org/10.1016/j.heliyon.2024.e25573.

Abbreviations

BLCA	bladder cancer
CNV	copy number variants
TCGA	The Cancer Genome Atlas
GEO	Gene Expression Omnibus
DRGs	disulfidptosis-related genes
PPI	protein-protein interaction
UMAP	uniform manifold approximation
K-M curve	Kaplan-Meier curve
GSVA	gene set enrichment analysis
DEGs	differentially expressed genes (DEGs)
GO	Gene Ontology
KEGG	Kyoto Encyclopedia of Genes and Genomes
ssGSEA	single-sample gene set enrichment analysis
IPS	immunophenotype scores
TCIA	The Cancer Immunome Atlas
IC50	half-maximum inhibitory concentration
LASSO	The Least Absolute Shrinkage and Selection Operator
OS	overall survival
ROC	receiver operating characteristic
TISCH	The Tumor Immune Single-Cell Hub
IHC	immunohistochemistry
HPA	The Human Protein Atlas database

References

[1] S. Li, K. Xin, S. Pan, Y. Wang, J. Zheng, et al., Blood-based liquid biopsy: insights into early detection, prediction, and treatment monitoring of bladder cancer, Cell. Mol. Biol. Lett. 28 (2023) 1–37, https://doi.org/10.1186/s11658-023-00442-z.

[2] A.M. Kamat, N.M. Hahn, J.A. Efstathiou, S.P. Lerner, P.-U. Malmström, et al., Bladder cancer. The Lancet 388 (2016) 2796–2810, https://doi.org/10.1016/S0140-6736(16)30512-8.

[3] J. Dobruch, M. Oszczudłowski, Bladder cancer: current challenges and future directions, Medicina 57 (2021) 749, https://doi.org/10.3390/medicina57080749.

[4] M. Wołącewicz, R. Hrynkiewicz, E. Grywalska, T. Suchojad, T. Leksowski, et al., Immunotherapy in bladder cancer: current methods and future perspectives, Cancers 12 (2020) 1181, https://doi.org/10.3390/cancers12051181.

[5] L. Zhou, G. Xu, F. Huang, W. Chen, J. Zhang, et al., Apoptosis related genes mediated molecular subtypes depict the hallmarks of the tumor microenvironment and guide immunotherapy in bladder cancer, BMC Med. Genom. 16 (2023) 1–14, https://doi.org/10.1186/s12920-023-01525-8.

[6] X. Zheng, H. Xu, T. Lin, P. Tan, Q. Xiong, et al., CD93 orchestrates the tumor microenvironment and predicts the molecular subtype and therapy response of bladder cancer, Comput. Biol. Med. 147 (2022) 105727, https://doi.org/10.1016/j.compbiomed.2022.105727.

[7] J.F. Kerr, A.H. Wyllie, A.R. Currie, Apoptosis: a basic biological phenomenon with wideranging implications in tissue kinetics, Br. J. Cancer 26 (1972) 239–257, https://doi.org/10.1038/bjc.1972.33.

[8] L. Galluzzi, I. Vitale, S.A. Aaronson, J.M. Abrams, D. Adam, et al., Molecular mechanisms of cell death: recommendations of the nomenclature committee on cell death 2018, Cell Death Differ. 25 (2018) 486–541, https://doi.org/10.1038/s41418-017-0012-4.

[9] D. Tang, R. Kang, T.V. Berghe, P. Vandenabeele, G. Kroemer, The molecular machinery of regulated cell death, Cell Res. 29 (2019) 347–364, https://doi.org/10.1038/s41422-019-0164-5.

[10] X. Liu, L. Nie, Y. Zhang, Y. Yan, C. Wang, et al., Actin cytoskeleton vulnerability to disulfide stress mediates disulfidptosis, Nat. Cell Biol. (2023) 1–11, https://doi.org/10.1038/s41556-023-01091-2, 10.1038/s41556-023-01091-2.

[11] T. Zheng, Q. Liu, F. Xing, C. Zeng, W. Disulfidptosis Wang, A new form of programmed cell death, J. Exp. Clin. Cancer Res. 42 (2023) 137, https://doi.org/10.1186/s13046-023-02712-2.

[12] L. Yang, W. Zhang, Y. Yan, Identification and characterization of a novel molecular classification based on disulfidptosis-related genes to predict prognosis and immunotherapy efficacy in hepatocellular carcinoma, Aging (Albany NY) 15 (2023) 6135, https://doi.org/10.18632/aging.204809.

[13] R. Saito, M.E. Smoot, K. Ono, J. Ruscheinski, P.-L. Wang, et al., A travel guide to Cytoscape plugins, Nat. Methods 9 (2012) 1069–1076, https://doi.org/10.1038/nmeth.2212.

[14] M.D. Wilkerson, D.N. Hayes, ConsensusClusterPlus: a class discovery tool with confidence assessments and item tracking, Bioinformatics 26 (2010) 1572–1573, https://doi.org/10.1093/bioinformatics/btq170.

[15] H. Wickham, ggplot2, Wiley interdisciplinary reviews: Comput. Stat. 3 (2011) 180–185, https://doi.org/10.1002/wics.147.

[16] T. Therneau, T. Lumley, R Survival Package, R Core Team, 2013.

[17] S. Hänzelmann, R. Castelo, J.G.S.V.A. Guinney, Gene set variation analysis for microarray and RNA-seq data, BMC Bioinf. 14 (2013) 1–15, https://doi.org/10.1186/1471-2105-14-7.

[18] M.E. Ritchie, B. Phipson, D. Wu, Y. Hu, C.W. Law, et al., Limma powers differential expression analyses for RNA-sequencing and microarray studies, Nucleic Acids Res. 43 (2015), https://doi.org/10.1093/nar/gkv007 e47-e47.

[19] M. Kanehisa, M. Furumichi, M. Tanabe, Y. Sato, K. Morishima, KEGG: new perspectives on genomes, pathways, diseases and drugs, Nucleic Acids Res. 45 (2017) D353–D361, https://doi.org/10.1093/nar/gkw1092.

[20] G. Yu, L.-G. Wang, Y. Han, Q.-Y. He, clusterProfiler: an R package for comparing biological themes among gene clusters, OMICS A J. Integr. Biol. 16 (2012) 284–287, https://doi.org/10.1089/omi.2011.0118.

[21] K. Yoshihara, M. Shahmoradgoli, E. Martínez, R. Vegesna, H. Kim, et al., Inferring tumour purity and stromal and immune cell admixture from expression data, Nat. Commun. 4 (2013) 2612, https://doi.org/10.1038/ncomms3612.

[22] D.A. Barbie, P. Tamayo, J.S. Boehm, S.Y. Kim, S.E. Moody, et al., Systematic RNA interference reveals that oncogenic KRAS-driven cancers require TBK1, Nature 462 (2009) 108–112, https://doi.org/10.1038/nature08460.

[23] P. Charoentong, F. Finotello, M. Angelova, C. Mayer, M. Efremova, et al., Pan-cancer immunogenomic analyses reveal genotype-immunophenotype relationships and predictors of response to checkpoint blockade, Cell Rep. 18 (2017) 248–262, https://doi.org/10.1016/j.celrep.2016.12.019.
[24] P. Geeleher, N.J. Cox, R.S. Huang, Clinical drug response can be predicted using baseline gene expression levels and in vitro drug sensitivity in cell lines, Genome Biol. 15 (2014) 1–12, https://doi.org/10.1186/gb-2014-15-3-r47.
[25] G. Sturm, F. Finotello, F. Petitprez, J.D. Zhang, J. Baumbach, et al., Comprehensive evaluation of transcriptome-based cell-type quantification methods for immuno-oncology, Bioinformatics 35 (2019) i436–i445, https://doi.org/10.1093/bioinformatics/btz363.
[26] B. Chen, M.S. Khodadoust, C.L. Liu, A.M. Newman, A.A. Alizadeh, Profiling tumor infiltrating immune cells with CIBERSORT, Cancer Systems Biology: Methods and Protocols (2018) 243–259, https://doi.org/10.1007/978-1-4939-7493-1_12, 10.1007/978-1-4939-7493-1_12.
[27] D. Maeser, R.F. Gruener, R.S. Huang, oncoPredict: an R package for predicting in vivo or cancer patient drug response and biomarkers from cell line screening data, Briefings Bioinf. 22 (2021) bbab260, https://doi.org/10.1093/bib/bbab260.
[28] F. Pontén, K. Jirström, M. Uhlen, The human protein atlas—a tool for pathology, J. Pathol.: A Journal of the Pathological Society of Great Britain and Ireland 216 (2008) 387–393, https://doi.org/10.1002/path.2440.
[29] D. Sun, J. Wang, Y. Han, X. Dong, J. Ge, et al., TISCH: a comprehensive web resource enabling interactive single-cell transcriptome visualization of tumor microenvironment, Nucleic Acids Res. 49 (2021) D1420–D1430, https://doi.org/10.1093/nar/gkaa1020.
[30] N. Ismaili, M. Amzerin, A. Flechon, Chemotherapy in advanced bladder cancer: current status and future, J. Hematol. Oncol. 4 (2011) 1–11, https://doi.org/10.1186/1756-8722-4-35.
[31] S. Liu, X. Chen, T. Lin, Emerging strategies for the improvement of chemotherapy in bladder cancer: current knowledge and future perspectives, J. Adv. Res. 39 (2022) 187–202, https://doi.org/10.1016/j.jare.2021.11.010.
[32] M. Wu, J. Gu, R. Guo, Y. Huang, M. Yang, Structure of mammalian respiratory supercomplex I1III2IV1, Cell 167 (2016) 1598–1609, https://doi.org/10.1016/j.cell.2016.11.012, e1510.
[33] M.R. Kwon, J.H. Lee, J. Park, S.S. Park, E.J. Ju, et al., NCK-associated protein 1 regulates metastasis and is a novel prognostic marker for colorectal cancer, Cell Death Discovery 9 (2023) 7, https://doi.org/10.1038/s41420-023-01303-6.
[34] R. El Ansari, M.L. Craze, M. Diez-Rodriguez, C.C. Nolan, I.O. Ellis, et al., The multifunctional solute carrier 3A2 (SLC3A2) confers a poor prognosis in the highly proliferative breast cancer subtypes, Br. J. Cancer 118 (2018) 1115–1122, https://doi.org/10.1038/s41416-018-0038-5.
[35] J. Ding, J. Xu, Q. Deng, W. Ma, R. Zhang, et al., Knockdown of oligosaccharyltransferase subunit ribophorin 1 induces endoplasmic-Reticulum-Stress-Dependent cell apoptosis in breast cancer, Front. Oncol. (2021) 4434, https://doi.org/10.3389/fonc.2021.722624.
[36] V. Kimonis, R. Al Dubaisi, A.E. Maclean, K. Hall, L. Weiss, et al., NUBPL mitochondrial disease: new patients and review of the genetic and clinical spectrum, J. Med. Genet. 58 (2021) 314–325, https://doi.org/10.1136/jmedgenet-2020-106846.
[37] A. Iuso, S. Scacco, C. Piccoli, F. Bellomo, V. Petruzzella, et al., Dysfunctions of cellular oxidative metabolism in patients with mutations in the NDUFS1 and NDUFS4 genes of complex I, J. Biol. Chem. 281 (2006) 10374–10380, https://doi.org/10.1074/jbc.M513387200.
[38] Y. Ni, M.A. Hagras, V. Konstantopoulou, J.A. Mayr, A.A. Stuchebrukhov, et al., Mutations in NDUFS1 cause metabolic reprogramming and disruption of the electron transfer, Cells 8 (2019) 1149, https://doi.org/10.3390/cells8101149.
[39] J.-C. Kuo, Focal adhesions function as a mechanosensor, Progress in molecular biology and translational science 126 (2014) 55–73, https://doi.org/10.1016/B978-0-12-394624-9.00003-8.
[40] J.A. Smart, J.E. Oleksak, E.J. Hartsough, Cell adhesion molecules in plasticity and metastasis, Mol. Cancer Res. 19 (2021) 25–37, doi: 10.1158/1541-7786.MCR-20-0595.
[41] L. Wu, W. Lian, L. Zhao, Calcium signaling in cancer progression and therapy, FEBS J. 288 (2021) 6187–6205, https://doi.org/10.1111/febs.16133.
[42] Focal adhesion signaling and therapy resistance in cancerI Eke, N Cordes (Eds.), in: SEMIN CANCER BIOL, Elsevier, 31, 2015, pp. 65–75, https://doi.org/10.1016/j.semcancer.2014.07.00.
[43] S. Tan, D. Li, X. Zhu, Cancer immunotherapy: pros, cons and beyond, Biomed. Pharmacother. 124 (2020) 109821, https://doi.org/10.1016/j.biopha.2020.109821.
[44] D. Song, T. Powles, L. Shi, L. Zhang, M.A. Ingersoll, et al., Bladder cancer, a unique model to understand cancer immunity and develop immunotherapy approaches, J. Pathol. 249 (2019) 151–165, https://doi.org/10.1002/path.5306.
[45] M.R. Junttila, F.J. De Sauvage, Influence of tumour micro-environment heterogeneity on therapeutic response, Nature 501 (2013) 346–354, https://doi.org/10.1038/nature12626.
[46] A.A. Alizadeh, V. Aranda, A. Bardelli, C. Blanpain, C. Bock, et al., Toward understanding and exploiting tumor heterogeneity, Nat. Med. 21 (2015) 846–853, https://doi.org/10.1038/nm.3915.
[47] T.F. Gajewski, H. Schreiber, Y.-X. Fu, Innate and adaptive immune cells in the tumor microenvironment, Nat. Immunol. 14 (2013) 1014–1022, https://doi.org/10.1038/ni.2703.
[48] N.M. Anderson, M.C. Simon, The tumor microenvironment, Curr. Biol. 30 (2020) R921–R925, https://doi.org/10.1016/j.cub.2020.06.081. Fig 1.